Application of material point method to bearing capacity problems of shallow foundations

Takatoshi Kiriyama[1] and Y. Higo[2]

[1] Institute of Technology, Shimizu Corporation, 3-4-17, Etchujima, Koto-ku, Tokyo, 135-8530, Japan.
[2] Kyoto University, C-cluster, Katsura, Nishikyo-ku, Kyoto, 615-8540, Japan.

ABSTRACT

Strain localization takes place during the deformation of geomaterials. Simulations of geomaterial behavior must use numerical methods that can handle and simulate this specific geomaterial characteristic. In particular, when simulating geomaterials under large deformations, mesh tangling often occurs with mesh-based numerical methods such as the finite element method (FEM). The authors focus on this difficulty and employ a particle-based method, specifically the material point method (MPM), instead of FEM to avoid meshing and achieve simulations that are numerically robust. Various interpolation functions for MPM are proposed and their characteristics are discussed and compared through numerical examples focusing on bearing capacity problems of shallow foundations.

Keywords: Material Point Method, Shallow Foundation, Bearing Capacity

1 INTRODUCTION

Experimental and numerical investigations relating to shallow foundations, such as raft foundations, can be found in the literature. In order to verify the effectiveness of MPM when applied to bearing capacity problems related to shallow foundations, numerical examples are performed under small deformations and the results are compared with the theoretical Prandtl solution and simulations by a mesh-based method (the finite difference method, FDM). These comparisons verify the numerical accuracy of MPM. Analyses involving large deformations are then performed and discussed in terms of load-settlement relationships.

2 NUMERICAL METHOD

It has been reported that numerical oscillations occur in the original formulation of MPM when particles cross numerical grids (Bardenhagen and Kober 2004). Bardenhagen and Kober proposed a new method in which an interpolation function takes into account the controlling domain of each particle. This derivative interpolation function overcomes the numerical oscillation problem and is called the generalized interpolation material point (GIMP) method. There are two variants of the GIMP method. One is the contiguous particle GIMP (cpGIMP) method, in which particles domains are updated following their deformation in the axial direction. The other is unchanged/uniform GIMP (uGIMP) method, in which particles retain their initial controlling domains. More recently, Sadeghirad et al. enhanced the GIMP method, proposing the convected particles domain interpolation (CPDI) method in which particle domains deform as a parallelogram in 2D (Sadeghirad et al. 2011). The CPDI method was revised further by Sadeghirad et al. to become the CPDI2 method, in which particle domains deform as quadrilaterals in 2D (Sadeghirad et al. 2013). The differences among the various MPM interpolation functions are illustrated in Fig.1.

MPM was formulated originally as a dynamic explicit method. In order to apply MPM to static equilibrium problems such as load-settlement relationships, the dynamic relaxation method is employed. With this method, the damping force is as given by equation (1). The convergence criteria are shown as equation (2).

$$f_g^{damp,k} = -\alpha \cdot abs(f_g^{drive,k}) \cdot sign(v) \tag{1}$$

$$f_g^{drive,k} = f_g^{int,k} + f_g^{ext,k}$$

$$force\ \ ratio = abs\left(\sum f_g^{drive,k} / \sum f_g^{drive,ini}\right) < \varepsilon \tag{2}$$

in which, $f_g^{damp,k}$, $f_g^{drive,k}$, $f_g^{int,k}$, $f_g^{ext,k}$ are damping force, driving force (equal to the force imbalance between internal and external force), internal force, and external force at time step *k*, respectively. α is the damping factor and *sign* is the function that returns the sign of the arguments. *k* and *ini* are superscripts representing time step *k* and the initial state, respectively. The damping force acts in the opposite direction to the grid point velocity at the same magnitude (of α times the driving force). As the

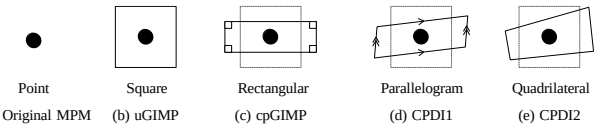

Fig.1. Differences among various MPM interpolations

simulation steps through the numerical process, the driving force decreases. Convergence is reached when the criteria in equation (2) are satisfied.

In the analyses that follow, the settlement reached after the convergence procedure above is called the equilibrium solution.

3 ANALYTICAL MODEL AND CONDITIONS

Analytical studies on bearing capacity problems of shallow foundations have been reported literally by Chen and Mizuno 1990 and Bui et al. 2008. Chen and Mizuno employed FEM to model small deformations, while Bui et al. adopted smooth particle hydrodynamics using the same analytical model as Chen and Mizuno but with large deformations. In this work, the analytical model and conditions described in Fig.2 and Table 2 are used in reference to these earlier studies. Pressure is applied to the surface grid points under the foundation in the small deformation cases. The loading block is employed to enforce tractions in the large deformation cases because the surface boundary changes during the simulation, making it difficult to apply a constant pressure. The density of the loading block is changed once the equilibrium condition has been satisfied at each loading stage in order to simulate incremental loading. The contact pressure under the loading block is not uniformly distributed. The average contact pressure is used to calculate the load-settlement relationships, where vertical displacement at the left (symmetrical center) is taken to be the settlement.

4 ANALYTICAL RESULTS

Load-settlement relationships for both small and large deformation cases and the time-history of unbalanced force ratio (equation (2)) are shown in Fig.3 and Fig.4, respectively. Fig.5 shows maximum shear strain distribution at each of the focused time steps shown in Fig.3 under small deformation. Fig.6 shows the same plots under large deformation for the various MPM interpolation methods.

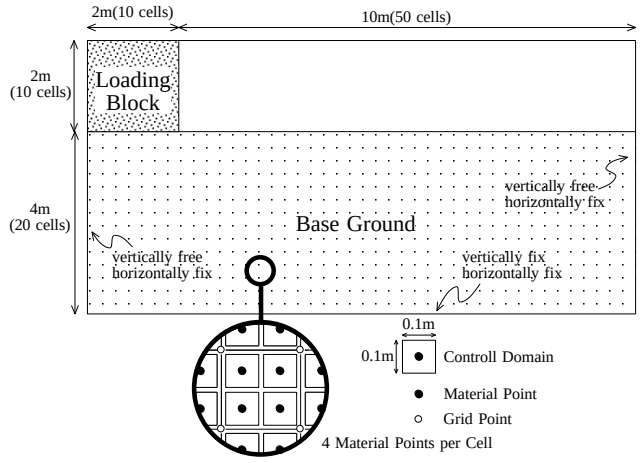

Fig.2. Analysis model.

In Fig.3 numerical results obtained by the finite difference method and Prandtl's solution ($q=c(\pi+2)=257$(kPa)) are also plotted in order to verify the numerical result calculated by MPM. Points [1]-[5] and [i]-[iv] in Fig.3 correspond to the maximum strain distribution inside the base ground shown in Fig.5 and Fig.6, respectively. Particles are illustrated and colored on their controlling domains described in Fig.1.

Fig.4 shows the time-history of driving force, indicating how the difference between external and internal forces reaches convergence. Convergence is reached within relatively fewer cycles when the ground behavior is elastic (Fig.4(b)). The source of the force imbalance (driving force) is mainly the rise in external force. As the external force increases further, the base ground begins to exhibit plastic behavior. In the plastic regime, more cycles are required to come to convergence because the driving force is increased by the generation of a force imbalance in the plastic state particles. In the ultimate state, yet more cycles are needed to reach convergence.

Looking at the analytical results for the small deformation cases, Fig.3(a) shows that the load-settlement relationship is in good agreement with that obtained by FDM and the ultimate bearing capacity is the same as given by Prandtl's solution. Fig.3(a) and point [1] in Fig.5 show the base ground behaving as elastic body and shear strain localizations are not observed. Point [2] in Fig.5 is where the base ground begins to show plasticity. Strain localization occurs under the foundation and a Kurdjumoff area (punching wedge) is formed. Point [3] in Fig.5 shows a non-linear response coming into play and strain localization extends beyond the base. The state shown in [4] is the theoretical ultimate state. In Fig.5, two shear band candidates are visible (s1 and s2 in Fig.5[4]). One is shallower and the other deeper. The shallow shear band 's1' grows and ultimately becomes the strain localization at the final state [5]. This final strain localization is in the same position as assumed in Prandtl's solution.

Table 1 Material properties.

Domain	E (kPa)	ν	ρ (g/cm^3)	c (kPa)	ϕ (deg)	ψ (deg)
Base Ground	20000	0.45	1.7	50	0.0	0.0
Loading Block	200000	0.3	10to300by10	-	-	-

Table 2 Analysis conditions.

Items	Values
Particles per cell	4
Dimensions(H x W)	6 m x 12 m
Width of cell	0.2 m
Time increment	0.00025
Damping factor	0.8
Convergence criteria	0.0001
Interpolation	uGIMP,cpGIMP,CPDI2
Number of Material Points	
Base Ground	4,800
Loading Block	400

Next, considering the analytical results for the large deformation cases, in Fig.6 the results for point [i] show that the base ground is acting as an elastic body, as seen in the small deformation cases, and strain localization does not occur. At point [ii] in Fig.6 there is visually recognizable deformation, while a clear increase in settlement appears in the load-settlement relationship in Fig.3(b). This is regarded as the ultimate bearing capacity in the large deformation cases. Strain localization is seen to occur at point [ii], where it spreads along the bottom of ground model and corresponds to 's2' seen in Fig.5[4]. At point [iii] a shear band begins to form from the bottom of the loading block to the ground surface; the load-settlement relationship at this point is a straight line with settlement resulting from the load increase as the base ground continues to fail. At point [iv], the loading block has reached almost the bottom of the modeled ground. The external force is in equilibrium with the bottom reaction and no more shear failure occurs.

Finally, the characteristics of the various interpolation functions are discussed based on the results given in Fig.6. In the case of uGIMP, because the controlling domains of particles are not updated, particles move in space within their initial controlling domains. As for cpGIMP, the controlling domains are updated in the axial direction (e.g. in the x-y direction in two dimensions). Particles can deform down to almost zero on the compression side while they expand up to the width of the numerical grid on the extension side. With CPDI2, particles are capable of deforming in any direction while maintaining continuity with neighboring particle domains. Although there are differences among these interpolation functions, the transfer of external forces to each particle takes place via a numerical grid. The equation of motion is satisfied as an agglomeration of particles. The load-settlement relationships in Fig.3 show that CPDI2 results in a larger bearing capacity than uGIMP and cpGIMP. This

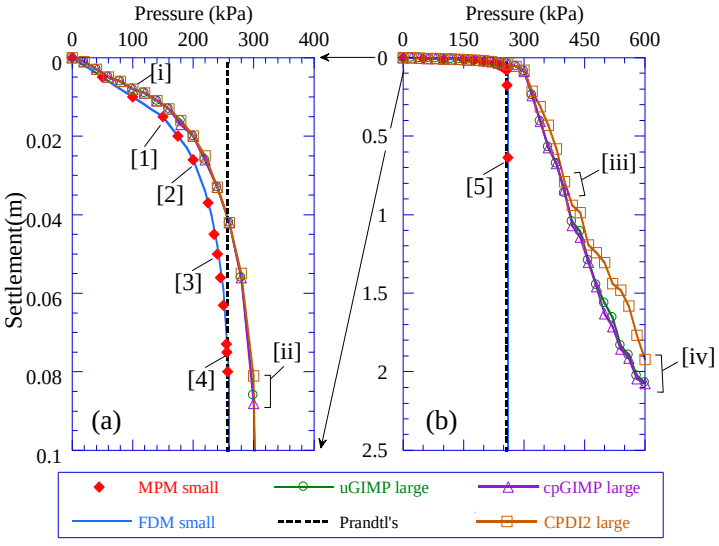

Fig.3. Load-settlement relationships: (a) Settlement range from 0(m) to 0.1(m); (b) Settlement range from 0(k) to 2.5(m).

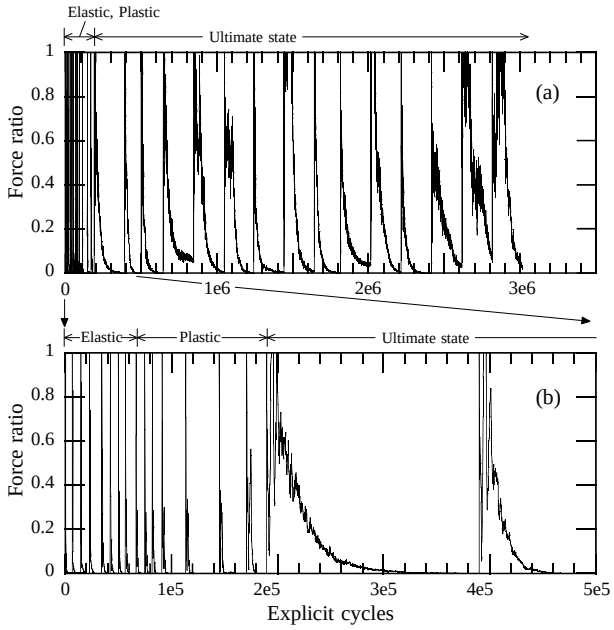

Fig.4. Example of driving force history under large deformation: (a) Complete history; (b) Same history up to first two cycles after reaching the ultimate state.

is because of the continuity of domains, which is realized only by the CPDI2 method. With uGIMP and cpGIMP, discontinuities in bearing capacity are clear in Fig.6 in the area neighboring the loading block. As such discontinuities occur more often between particles, the number of particles resisting the external force decreases. The number of particles in CPDI2 calculation is more than those of the other two methods.

Thus, differences in bearing capacity arising from the use of different interpolation functions arise from the way that forces transfer with the different particle domains. Geomaterials naturally have little resistance to tension and shear deformation is readily localized. In attempts to numerically forecast deformation, an interpolation function should be chosen depending on material behavior. For example, uGIMP and cpGIMP

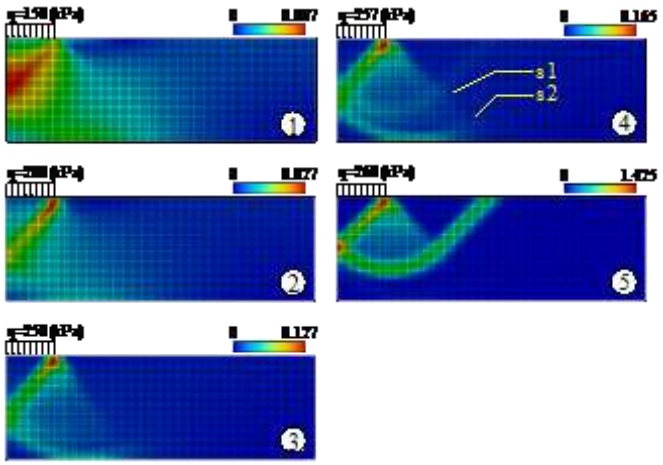

Fig.5. Distribution of maximum shear strain inside the ground under small deformation. The numbers correspond to the points marked in Fig.3.

should be employed for phenomena that include discrete behaviors while CPDI2 should be employed for phenomena without discrete behaviors.

3 CONCLUSION

In this paper characteristics of these functions are discussed and compared. The applicability and effectiveness of each interpolation function are also discussed, focused on bearing capacity problems of shallow foundation.

REFERENCES

Bardenhagen, S.G. and Kober, E.M. (2004). The generalized interpolation material point method, CMES, Vol.5, No.6, pp.447-495.

Bui, H., Fukagawa, R., Sako, K. and Ohno, S. (2008). Lagrangian mesh-free particles method (SPH) for large deformation and failure flows of geomaterial using elastic–plastic soil constitutive model, Int. J. Numer. Anal. Meth. Geomech., Vol.32, No.12, pp. 1537–1570.

Chen and Mizuno (1990). Nonlinear Analysis in Soil Mechanics: Theory and Implementation. Elsevier: Amsterdam.

Sadeghirad, A., Brannon, R.M. and Burghardt, J. (2011). A convected particle domain interpolation technique to extend applicability of the material point method for problems involving massive deformations, Int. J. Numer. Meth. Engng, Vol.86, No.12, pp.1435–1456.

Sadeghirad, A., Brannon, R.M. and Guilkey, J.E. (2013). Second-order convected particle domain interpolation (CPDI2) with enrichment for weak discontinuities at material interfaces, Int. J. Numer. Meth. Engng, Vol.95, No.11, pp.928–952.

Sulsky D., Chen, Z. and Schreyer, H.L. (1994). A particle method for history-dependent materials, Comput. Methods Appl. Mech. Engrg., Vol.118, pp.179-196.

Tatsuoka, F., Okahara, M., Tanaka, T. Tani, K. Morimoto, T. and Mohammed, S.A. (1991). Progressive failure and particle size effect in bearing capacity of a footing on sand, Geotechnical Engineering Congress, Vol.2, pp.788-802.

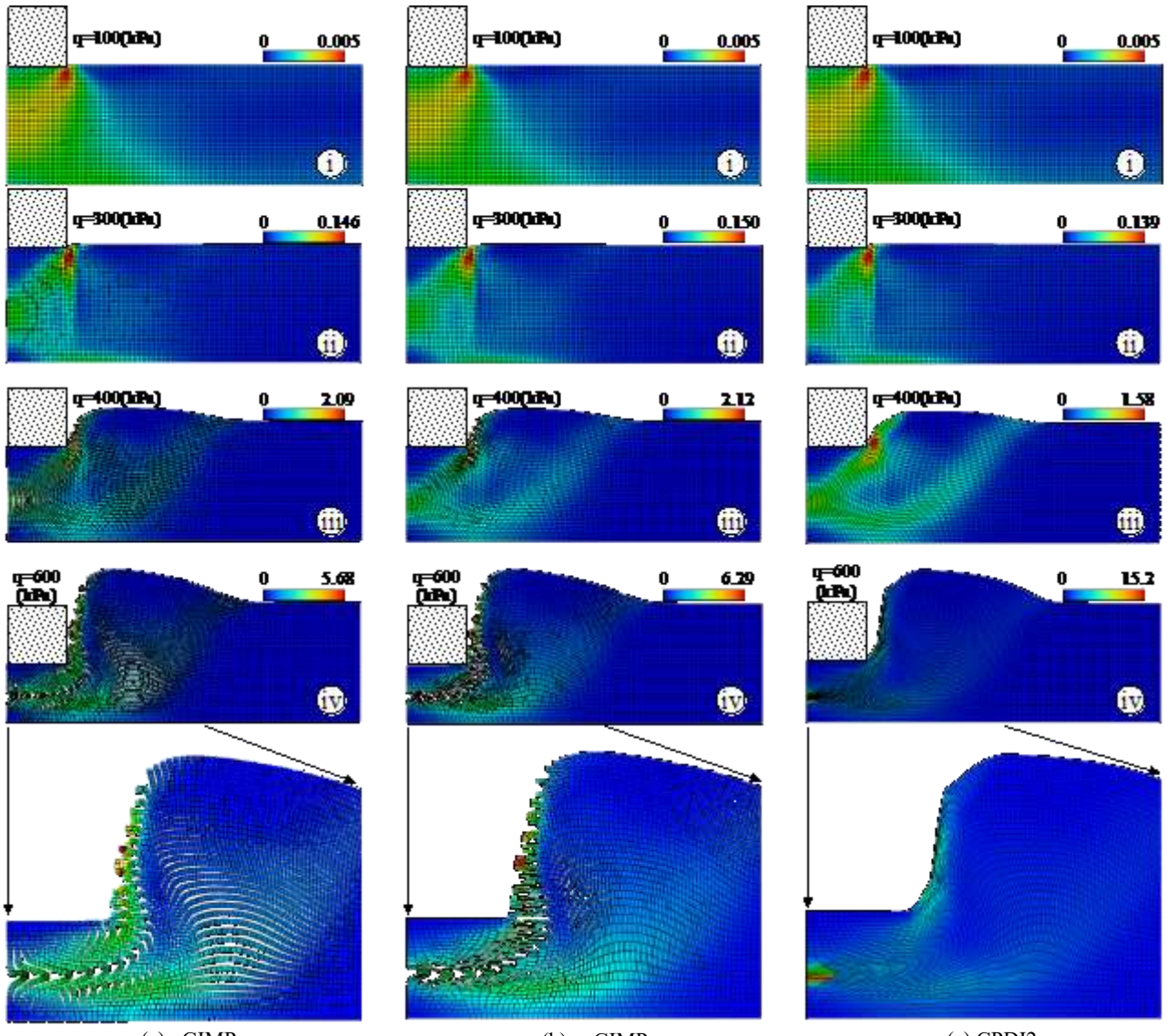

(a) uGIMP (b) cpGIMP (c) CPDI2

Fig.6. Distribution of maximum shear strain inside the ground under large deformation. The numbers correspond to the points marked in Fig-3. (a) uGIMP ground deformed with uniform square particles, showing many void domains among particles; (b) cpGIMP ground deformed with rectangular particles, still showing many voids among particles; each particle deforms according to the axial strain; (c) CPDI2 ground deformed with quadrilateral particles, showing no voids inside the ground.